RF Field Profiling Through Element Design for High Field Volume Coils

C. Akgun[1], L. DelaBarre[1], C. J. Snyder[1], G. Adriany[1], A. Gopinath[2], K. Ugurbil[1], and J. T. Vaughan[1]
[1]University of Minnesota-Center for Magnetic Resonance Research, Minneapolis, MN, United States, [2]University of Minnesota-Department of Electrical and Computer Engineering, Minneapolis, MN

Background:

The multi-channel volume coil can be comprised of an array of transmission line elements that are mutually decoupled and operated as independent coils in typically multiple-channel transmit and receive configurations[1-3]. In these designs, microstrip transmission elements have been implemented as magnetic field propagating elements.[4, 5] However, at high fields, short in vivo wavelengths and greater sample losses lead to RF in-homogeneities and RF inefficiencies. Optimization of these elements are required to overcome these challenges for desired MR applications, e.g. spectroscopy requires peak B1+ in a focal region of interest while applications like diffusion tensor imaging (DTI) requires whole brain coverage. In this study, two different microstrip designs with varying impedance lines -- one producing peak B1+ in the center and the other extending the length of usable B1+ along the length of the coil-- are investigated. Simulation and image results for 8-channel volume coils incorporating these element designs were obtained using a phantom at 7T.

Concept:

A capacitively terminated microstrip transmission line produces a standing wave with a current distribution peaking at the center of the line. To produce a greater peak B1+ at the center of the coil or to extend the coaxial B1+ field, the signal line was patterned into repeating thick and thin sections (Fig. 1a, b). By varying impedances along the line, the current density along the length of the transmission line is controlled; current can be peaked with a 3 section design (Fig. 1a) or broadened with a 7 section microstrip design (Fig. 1b).

Methods:

Three eight-channel transceiver arrays were built (Fig. 1b). Each element was comprised of a low loss Teflon substrate (ε_r = 2.08) with height and length of 1.90 cm and 14.0 cm, respectively. The elements were attached to a cylindrical plexi-glass shell 25.4 cm in diameter and 14.0 cm in length. The conductor widths were alternated with 1.2 cm copper tape and 16 gauge copper wire (0.127 cm diameter) for the *3 section elements* (2 tape and 1 wire section) and *7 section elements* (4 tape and 3 wire sections), while the standard straight microstrip element had only 1.2 cm copper tape. Each element was individually tuned to 297 MHz (7 T) and matched to a 50-Ω, coaxial cable. Decoupling capacitors between nearest neighbors were not incorporated. Also, the phantom (cylindrical 8-liter sucrose/saline phantom (ε_r = 58.1, σ = 0.539 (S/m)) was positioned at the same location for each experiment. Experiments were performed in a 7 T (ω_o = 297 MHz) magnet (Magnex Scientific, UK) interfaced to a Siemens console (Siemens HealthCare, Germany).

Numerical Maxwell solutions of the 8-channel transceiver arrays were calculated about a sucrose/saline phantom (ε_r = 58.1, conductivity = 0.539 S/m) using xFDTD version 6.3 (Remcom Inc., State College, PA). Each channel was simulated individually and combined with 45 degree phase increments between neighboring elements using the principle of superposition into an 8 channel circular configuration in post-processing by Matlab (version 7.5).

Results:

The B1+ xFDTD simulations (Fig. 2a,b) show the 8-channel, *3 section element* coil performing 45% greater in the center of the coil (Fig. 2c) while the E-fields (Fig. 3a,b) are 30-40% less (transaxial plane) than the traditional microstrip coil indicating that the new design would have significantly lower SAR results (Fig. 3c). Experimentally, the *3 section element* coil performs 38% (Fig. 4b) greater in the center of the coil compared the microstrip while the *7 section element* coil performs roughly 24% greater in transaxial plane (Fig. 4c). In the sagittal B1+ maps, the *3 section element* has a pronounced circular excitation with a central peak (Fig. 5b); however, the *7 section* element has a larger extent of usable B1+ intensity in the center plane (Fig. 5c) compared to the microstrip element (Fig. 5a). The intrinsic SNR profiles are approximately equivalent for all designs indicating that the new designs do not suppress receive sensitivity (Fig. 6a, b, c).

Conclusions:

Novel alternating impedance element coils are introduced for high field imaging. The 3 section element demonstrated a much stronger peak B1+ profile in the center of the phantom compared to a standard, single-segment microstrip coil according to predictions and validating measurements. Simulations indicate higher B1+ and lower E-field in the field of view for a 3 section element when compared to the standard microstrip design. Images acquired demonstrate a larger extent of B1+ when altering the traditional microstrip line to a 7 section line. Alternating impedances in signal lines in multi-channel transceiver coils appear to be a good strategy for overcoming B1+ field inefficiencies and SAR limitations in high field MRI.

References:[1] Roemer PB, et al. Magn Reson Med 1990;16: 192-225, [2] Vaughan J.T. et al. Magn Reson Med 1994;32: 206-218, [3] Vaughan, J. ISMRM 2004 [4] Lee RF, et al. *Magn Reson Med* 2001; 45: 673-683 [5] Adriany,G, et al. Magn Reson Med 2005; 53(2): 434-445

Acknowledgements: This work was funded by Keck Foundation, NIH-NIBIB-EB000895, P30 NS057091, NIH NIBIB-EB006835, NIH-NIBIB-EB007327, and NIH-NCRR-P41-RR008079.

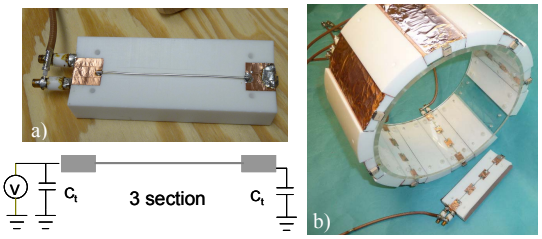

Fig. 1) **a)** 3 section microstrip element with 1 element circuit **b)** 8-channel 7 section microstrip volume coil with 1 element circuit

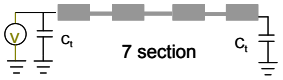

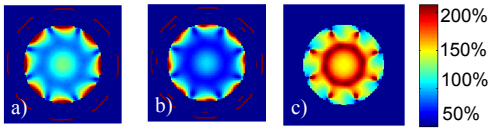

Fig. 2) 8-ch. B1+ *simulation* transaxial plot for **a)** 3 section microstrip **b)** for microstrip **c)** ratio of **a/b**

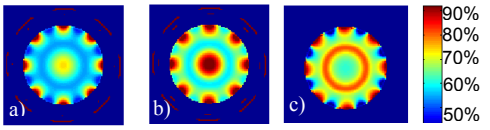

Fig. 3) 8-ch. E-field *simulation* transaxial plot **a)** 3 section microstrip **b)** for microstrip **c)** ratio of **a/b**

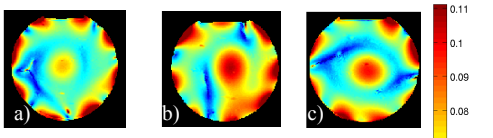

Fig. 4) 8-ch. Experimental transaxial B1+ maps for **a)** microstrip **b)** with 3 sections **c)** with 7 sections

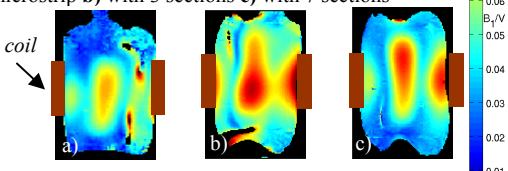

Fig. 5) 8-ch. Experimental sagittal B1+ maps **a)** microstrip **b)** with 3 sections **c)** with 7 sections

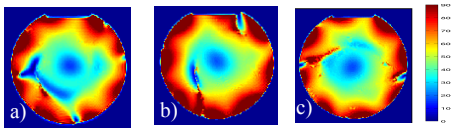

Fig. 6) 8-ch. transaxial ISNR **a)** microstrip **b)** with 3 sections **c)** with 7 sections